Electronic structure and magnetic properties of graphitic ribbons

L. Pisani,[1] J. A. Chan,[1] B. Montanari,[2] and N. M. Harrison[1,3]

[1]*Department of Chemistry, Imperial College London, South Kensington Campus, London SW7 2AZ, United Kingdom*
[2]*CCLRC Rutherford Appleton Laboratory, Chilton, Didcot, Oxfordshire OX11 0QX, United Kingdom*
[3]*CCLRC Daresbury Laboratory, Daresbury, Warrington WA4 4AD, United Kingdom*

First-principles calculations are used to establish that the electronic structure of graphene ribbons with zigzag edges is unstable with respect to magnetic polarization of the edge states. The magnetic interaction between edge states is found to be remarkably long ranged and intimately connected to the electronic structure of the ribbon. Various treatments of electronic exchange and correlation are used to examine the sensitivity of this result to details of the electron-electron interactions, and the qualitative features are found to be independent of the details of the approximation. The possibility of other stablization mechanisms, such as charge ordering and a Peierls distortion, are explicitly considered and found to be unfavorable for ribbons of reasonable width. These results have direct implications for the control of the spin-dependent conductance in graphitic nanoribbons using suitably modulated magnetic fields.

I. INTRODUCTION

Recently, room-temperature ferromagnetism has been reported for samples of highly oriented pyrolytic graphite that has been irradiated with high-energy protons.[1–3] These observations have fueled interest in the magnetic properties of carbon-only materials, which are of both great technological and fundamental importance. The experimental evidence gathered thus far indicates that the magnetism does not originate from d or f electrons provided by chemical impurities but states of s-p symmetry unpaired at structural defects.[4] The interest in s-p magnetism predates these recent discoveries,[5–7] and so does the interest in the technological exploitation of nanosized particles of graphite, or *nanographite*, which exhibit unusual features depending on their shape, surface termination, and applied field or pressure.[8] Their tunable and controllable properties open the way to implementing electromagnetic devices that are simultaneously high-tech, low-cost, and easy to process.

A graphitic ribbon, created by cutting a graphene sheet along two parallel lines, exhibits edges, which lower the dimensionality of the system and, if close enough to each other, produce a nanosized material. This system is particularly interesting from a theoretical point of view because the investigation of its properties as a function of width allows one to explore nanosize effects as well as bulk effects and the crossover between the two. Moreover, graphitic ribbons are of particular interest from the magnetic point of view as the presence of zigzag edges disrupts the diamagnetic delocalization of the graphitic π-electron system, creating an instability which can be resolved by stabilization via electronic spin polarization. Several theoretical studies employing the standard and/or extended tight-binding model,[11–14] renormalization-group technique,[15] and density-functional theory (DFT) (Refs. 9, 10, and 16) have been devoted to graphitic ribbons and indicate that both charge localization and paramagnetism occur in ribbons with zigzag edges.[17] Experimental evidence of a room-temperature paramagnetic response exists for activated carbon fibers consisting of disordered networks of minute graphitic fragments about $2-3$ nm across.[18–20] Very recent work using DFT within the

local spin-density approximation (LSDA) analyzes the electronic and magnetic properties of armchair and zigzag ribbons[10] and indicate the possibility of inducing a half metallic state in zigzag edges by applying an electric field.[9]

The current work addresses possible stabilization mechanisms for ribbons with zigzag edges and analyzes in detail the properties of the magnetically stabilized systems, suggesting the possibility of controlling the spin-dependent conductance with suitably modulated magnetic fields. This is achieved by computing the structural and electronic properties as a function of the ribbon's width. The method of choice for this work is hybrid exchange density functional in the B3LYP form.[21–23] The mixing of nonlocal and semilocal exchange present in hybrid-exchange functionals overcomes the major flaws of the LSDA (Ref. 24) and generalized gradient approximations (PBE) (Ref. 25) in the prediction of the correct electronic and magnetic ground state in strongly correlated electron systems.[26,27] Furthermore, they yield an improved quantitative description of thermochemistry,[28] optical band gaps,[29] magnetic moments and coupling constants,[30–35] and metal insulator transitions[36] in strongly interacting systems. This approach has also been used succesfully in recent studies of magnetic ordering in wide band-gap semiconductors,[37] Prussian blue analogs,[38] and in fullerene based metal-free systems.[38,39] It appears that the hybrid exchange approach allows the balance between electron localization and delocalization, which is crucial in the current work, to be described more reliably than in the LSDA and PBE. The authors, however, are not aware of a systematic study of the perfomances of B3LYP for systems containing localized (in the sense of nonbonding or atomic) orbitals of only s-p nature. The sensitivity of the calculated results to the treatment of electronic exchange and correlation is therefore explored by comparison with LSDA and PBE calculations. In addition to the magnetic stabilization, alternative mechanisms involving geometric distortion and charge polarization are also addressed.

The organization of this paper is as follows: in Sec. II the details of the system and of the computations are described. In Sec. III, the electronic structure of the nonmagnetic state and the eventuality of an instability with respect to the
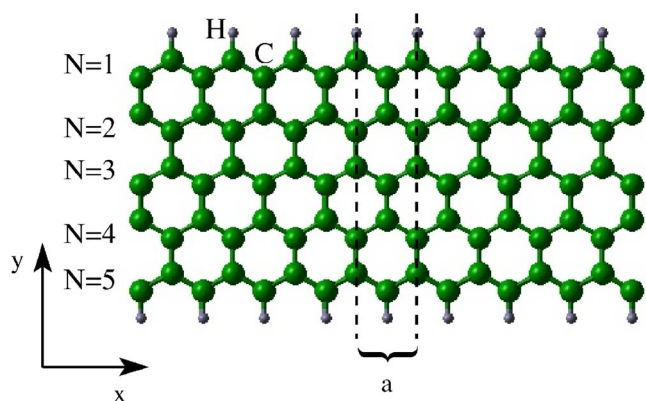
FIG. 1. (Color online) A monohydrogenated ribbon of width N =5 along y. The system is periodic only along x and the dashed lines delimit the periodic unit cell of length a.

electron-lattice interaction are discussed. In Sec. IV the possible magnetic states (para-, ferro-, and antiferromagnetic) and the strength of the exchange interaction as a function of the ribbon width are investigated. Before concluding in Sec. VI, Sec. V presents a preliminary study of the likelihood of a charge-polarized state as opposed to the spin-polarized one.

II. SYSTEM'S GEOMETRY AND COMPUTATIONAL DETAILS

A graphene ribbon of the type shown in Fig. 1 is obtained by cutting a graphene sheet along two parallel zigzag lines. The ribbon is periodic in the x direction only, and the unit cell is delimited by the dashed lines. The width of the ribbon along the nonperiodic dimension y is defined here by the number N of *trans*-polyacetylenelike rows of carbon atoms that run along x. Concerning the electronic structure of a ribbon, this work mainly investigates one type of termination for the dangling σ bonds at the edges: the monohydrogenated ribbon (Fig. 1 illustrates this ribbon structure for N=5). Concerning the magnetic properties, the study is extended to the cases of nonterminated and methylene group terminated ribbons, the latter being depicted in Fig. 2 (N=5), where the dangling σ bonds are saturated alternatively by a methylene group and a H atom (saturation with methylene groups only in a planar configuration is prohibited by the steric hindrance between adjacent methylene groups). In the monohydrogenated ribbon, the π electron states of the edge atoms are bound to appear closer to the Fermi level than the σ states, since the latter provide a stronger bonding interaction than the former. In the following the focus will be on these highest occupied states.

The first-principles calculations presented here have been performed using the hybrid exchange density functional B3LYP as implemented in the CRYSTAL package.[41] In CRYSTAL, the crystalline wave functions are expanded as a linear combination of atom centered Gaussian orbitals (LCAO) with s, p, d, or f symmetry. The calculations reported here are all-electron, i.e., with no shape approximation to the ionic potential or electron charge density.

The geometry optimizations are performed using the algorithm proposed by Schlegel *et al.*[42] The starting geometry
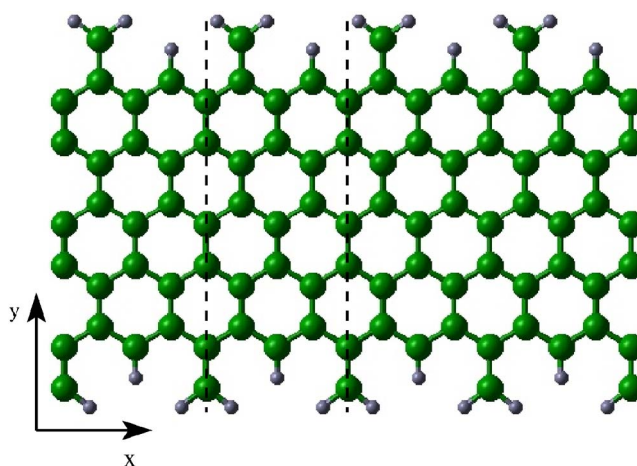

FIG. 2. (Color online) The N=5 ribbon with its zigzag edges terminated by an alternation of methylene groups and H atoms. The dashed lines represent the unit cell.

was determined by cutting a sheet of graphene optimized with B3LYP and saturating the dangling bonds with H atoms, with a C-H distance equal to that of B3LYP-optimized benzene. The optimization with B3LYP for graphene gave a lattice constant value of 2.460 Å, which is only 0.04% smaller than the experimental lattice constant of natural graphite and corresponds to C-C bond lengths of 1.420 Å. The B3LYP optimized C-H bond length of benzene is 1.093 Å, consistent with the experimental value of 1.080 Å.[43]

Basis sets of double valence quality ($6\text{-}21G^*$ for C and $6\text{-}31G^*$ for H) are used. A reciprocal space sampling on a Monkhorst-Pack grid of shrinking factor equal to 60 is adopted after finding it to be sufficient to converge the total energy to within 10^{-4} eV per unit cell. The Gaussian overlap criteria which control the truncation of the Coulomb and exchange series in direct space are set to 10^{-7}, 10^{-7}, 10^{-7}, 10^{-7}, and 10^{-14}. Typically linear mixing of 70% and an Anderson second-order mixing scheme is used to guide the convergence of the SCF procedure. Level shifting (typically by 0.3 a.u.) is sometimes required to converge the non-spin-polarized configuration.

In order to compare the energies of various magnetically ordered states, it is necessary to converge stable self-consistent field solutions for different electronic spin configurations. This is achieved by preparing a superposition of aligned or antialigned spin densities for particular atomic states to provide a suitable initial wave function. It is important to note that this only affects the initial wave functions and that all solutions presented are unconstrained and self-consistent.

III. NONMAGNETIC STATE

A. Electronic band structure and density

In this section, the properties of the nonmagnetic state of a monohydrogenated ribbon of width N=10 are discussed. Ribbons with the other terminations considered here and of different width show a qualitatively similar behavior and will therefore not be discussed in detail. Figure 3 shows the band
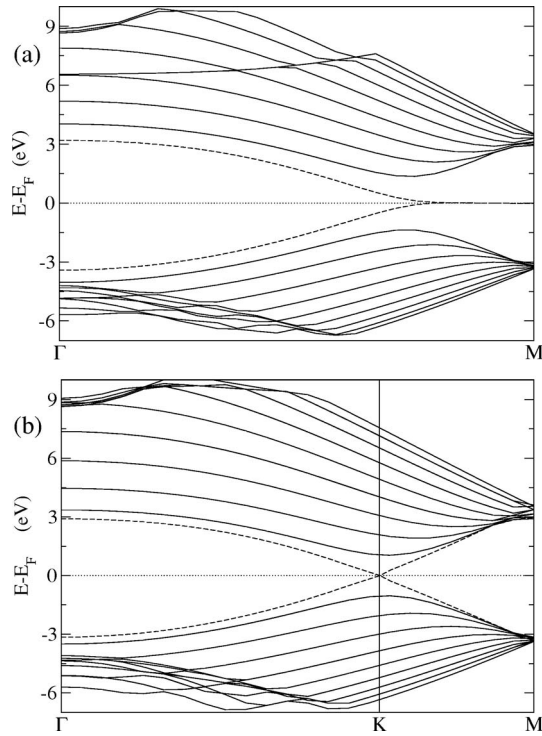
FIG. 3. Relevant portion of the electronic band structure of (a) a nonmagnetic, $N=10$, monohydrogenated ribbon, and (b) a graphene sheet represented in the unit cell of the ribbon. Dashed lines represent "edge" bands and the dotted line is at the Fermi level.
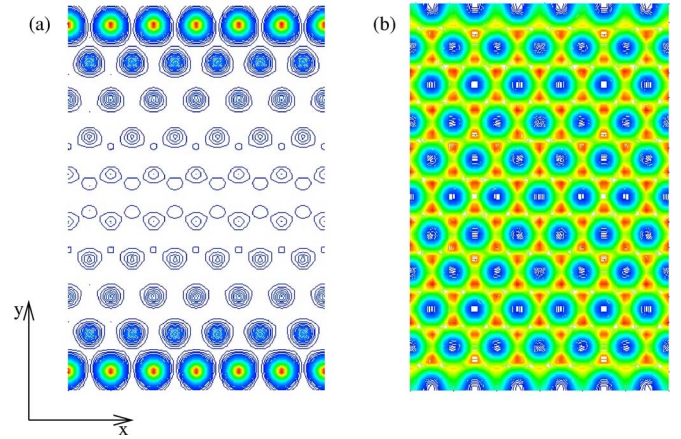

FIG. 4. (Color online) Electron density of a nonmagnetic, mono-hydrogenated, $N=10$ ribbon contributed by (a) the states near the Fermi level and (b) the rest of the occupied π states. The range of isovalues is $[0:0.028]e/\text{Å}^3$ in case (a) and $[0:0.12]e/\text{Å}^3$ in case (b).

structure of (a) the ribbon compared to that of (b) an infinite graphene sheet projected onto the ribbon's first Brillouin zone. The most striking difference between (a) and (b) affects the highest occupied and the lowest unoccupied band, represented with dashed lines. The shape of these two bands in (a) and (b) is similar between $k=0$ and $k=2\pi/3a$ but becomes markedly different between $k=2\pi/3a$ and $k=\pi/a$ (M). In the case of graphene, (b), the two bands become degenerate at E_F at a single point, which is equivalent to the K point (point at which the semimetallic zero gap appears) in the first Brillouin zone of graphene, and then diverge from each other between K and $k=\pi/a$. In the case of the ribbon, the two bands converge until they become degenerate exactly at E_F (and the k point at which this happens depends on the ribbon's width),[44] and they remain degenerate and totally dispersionless until $k=M$. This results in a high density of states at E_F and this electronic structure suggests an instability that might be resolved by a number of mechanisms including (i) a geometric distorsion, (ii) electronic spin polarization, (iii) electronic charge polarization. The likelihood of each of these eventualities will be investigated in this work.

By plotting the electron density from states with an energy falling in a small interval below the Fermi level, the location of the dispersionless states at E_F within the ribbon can be visualized. By choosing an energy interval of 0.4 eV, the charge density map in Fig. 4(a) is obtained. The electron density is localized mostly at the edges, with the peaks corresponding to the location of the C atoms at the edges, and decays into the bulk of the ribbon. In the following therefore the two dashed bands will be referred to as the "edge" bands.

Notably, due to the topology of the lattice, the atoms of the two edges belong to different sublattices of the bipartite graphene lattice and therefore the degenerate orbitals at E_F interpenetrate in a nonbonding network. Within a tight-binding model, Fujita *et al.*[11] have shown that nonbonding orbitals alone form the dispersionless part of these bands. At $k=M$ the states are fully localized at the edges and as k approaches Γ they penetrate into the bulk.

In contrast, projection onto the rest of the occupied bands in Fig. 3(a) produces the charge density plot in Fig. 4(b). The electronic charge contributed by these states is distributed across the whole ribbon, and does not decay. The highest values of this density correspond to the positions of the C atoms with the exception of the edge's atoms and is significant also along the C-C bonds, showing a strong bonding character. These states are in nature the same as the π bonding states in graphene and in the following they will be referred to as "bulk" bands.

B. Geometric distortion

As mentioned in the previous section, the high density of states at the Fermi level present in the nonmagnetic ribbons may indicate an instability with respect to a geometric distortion, which in this case would be a Peierls distortion as the system is one-dimensionally periodic.[45] The prototype system for a Peierls distortion is trans-polyacetylene which, interestingly, coincides with the $N=1$ monohydrogenated ribbon. It is therefore interesting to investigate whether also ribbons with $N\geq 2$ are unstable with respect to dimerization.

The nature of the electronic states at E_F in polyacetylene, however, is drastically different from those of a ribbon with $N\geq 2$.[46] By inspection of Fig. 3(a) all bulk bands appear to be nearly degenerate at $k=M$ (about 3 eV below the Fermi level). By applying a simple LCAO scheme to a ribbon with $N=5$ one obtains the description displayed in Fig. 5(a), where a wave function of those degenerate bulk bands is superimposed upon a wave function of the twofold degener-
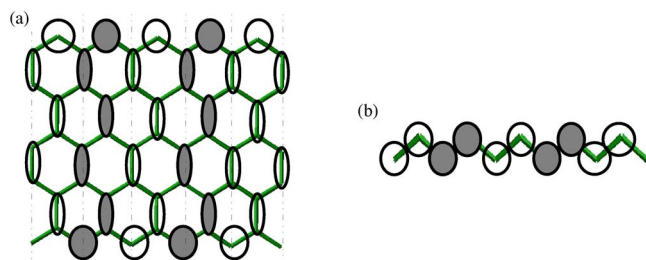
FIG. 5. (Color online) Wave-function symmetry at the $k=\pi/a$ point for a ribbon with $N=5$ (a) and for trans-polyacetylene (b). The circles represent nonbonding orbitals at the Fermi level while the ovals depict those bulk states that are about 3 eV below the Fermi level [see Fig. 3(a)]. The phase of the orbitals is represented by filled ($+$) and empty ($-$) symbols.
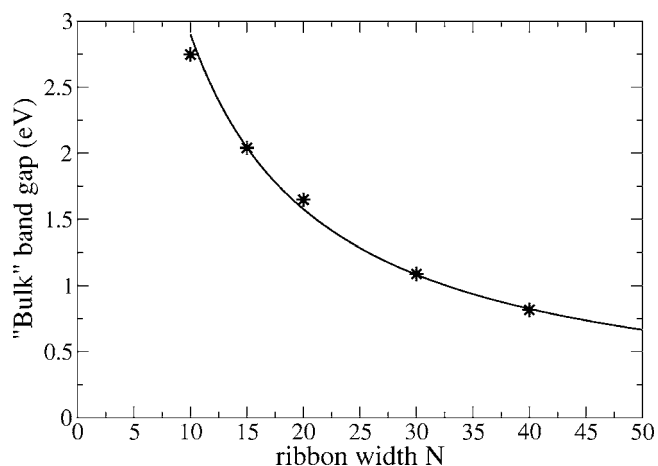

FIG. 6. The energy gap between the highest occupied and lowest unoccupied *bulk* states of a nonmagnetic, monohydrogenated ribbon as a function of the ribbon's width.

ate state at the Fermi level at M. Analogously, for the case of undistorted polyacetylene, Fig. 5(b) represents one of the possible wave functions of the twofold degenerate state at E_F. In polyacetylene, the nonbonding orbitals are located on nearest neighbors and thus may gain electronic stabilization energy by forming dimers with a consequent opening of a gap at the Fermi level. In the ribbon, the same orbitals are separated by sites in which orbitals participate in bulk states. In order for the edge states to dimerize the bulk bonding must be disturbed causing an energy loss which competes with the energy gained from dimerization. The energy cost of dimerization increases with ribbon thickness and therefore one expects dimerization to be suppressed at some critical ribbon width. Our fully relaxed, first-principles calculations prediction of a bond alternation length along the polyacetylenelike chain at the edge is 0.027 Å for $N=2$ and smaller than 0.001 Å for $N=3$. The sharp decrease of the magnitude of the dimerization with N is a measure of the rigidity of the underlying $\sigma-\pi$ bonding structure.

Full structural relaxation of the $N=10$, monohydrogenated ribbon confirms the absence of a dimerization distortion but at the same time a lattice distortion occurs due to an edge relaxation effect. To describe the topology of the relaxation we adopt the view in which the ribbon is made up of polyacetylenelike chains linked by rungs. A carbon atom in the bulk has two intrachain bonds and one interchain (rung) bond with its nearest neighbors; at the edge only intrachain bonds are present. The edge relaxation consists of a uniform contraction (by 0.02 Å in the case of $N=10$) of the intrachain bonds at the edge and a consequent expansion of the interchain rungs. This effect decreases sharply moving away from the edge and is to be ascribed to the accumulation of extra bonding charge (with respect to the bulk π bonds) at the nonbonding part of the π orbital at the edge. Contrary to the Peierls distortion in polyacetylene, not all the nonbonding charge at the edge participates in this extra bonding due to the lack of a bonding counterpart at the atom involved in an interchain bond. Crucially this establishes that the localized nonbonding charge persists at the edge even after surface relaxation, mantaining its tendency towards a magnetic state, as will be shown in Sec. IV.

C. Very wide ribbons and the graphene limit

As the width of the ribbon increases, it is expected that its bulk bands, as defined in Sec. III A, will recover the graphene limit and the gap between the bulk occupied and bulk unoccupied states will eventually close. For $N\to\infty$, the edge bands, sandwiched between the bulk bands, will become degenerate, with an energy equal to E_F, at $k=\frac{2}{3}\frac{\pi}{a}$ (K). It is therefore interesting to determine the ribbon's width at which the band gap between the bulk states in a ribbon closes. By extrapolating the data in Fig. 6, this gap is found to recover the graphite limit of a zero band gap, within the room-temperature thermal energy, when the ribbon width is $\sim$0.25 μm. This result is independent of whether the geometry of the ribbons is constrained at the graphene geometry or fully relaxed. This critical width is very large, indicating that the screening of the perturbation caused by the presence of the edges is very slow compared to, for instance, the screening of an electronic perturbation at the surface of semiconducting crystals (typically around 10 nm). The much larger penetration depth in graphitic ribbons could be related to the large delocalization energy (hopping parameter t $\simeq$2.5 eV) typical of carbon aromatic systems, as well as to their dimensionality. Unusually long-ranged surface effects have been found in previous studies of graphitic systems. In a combined atomic force microscopy–scanning tunnel microscopy study, Ruffieux *et al.* observed electronic polarization effects extending over a range of 50–60 nm when H was adsorbed on graphite.[47] In a diamagnetic susceptibility study,[17] it was found that the slope of the orbital susceptibility as a function of the ribbon width depends on whether it has a zigzag or armchair geometry. Surprisingly, the difference between the slope in the two cases was observed to increase with the ribbon's width.

The long-ranged nature of these effects indicates that in the graphene ribbon a small concentration of defects would be enough to drastically alter the semimetallicity and the conducting properties of the material. This conclusion may also be tentatively extended to a wide range of graphitic systems but the effects of the three-dimensional structure requires further investigation.
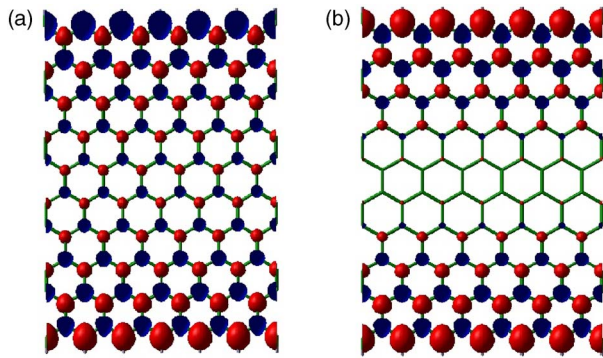
FIG. 7. (Color online) Isovalue surfaces of the spin density for the antiferromagnetic case (a) and ferromagnetic case (b). The dark grey (red online) surface represents spin up density and the black (blue online) surface spin down density. The range of isovalues is $[-0.28:0.28]\mu_B/\text{Å}^3$ in case (a) and $[-0.09:0.28]\mu_B/\text{Å}^3$ in case (b).

IV. ELECTRONIC SPIN POLARIZATION

A. Electronic band structure and density of states

As the analysis in Sec. III B excludes the possibility that a Peierls distortion can resolve the instability brought about by the high density of states at the Fermi level in the nonmagnetic ribbons, the eventuality of stabilization through spin polarization is investigated here.

By allowing the system to be spin polarized, stable magnetic states are found, whose spin density is shown in Figs. 7(a) and 7(b). Here, the state depicted in Fig. 7(a) is referred to as *antiferromagnetic* (AF) because the spin moments on the C atoms on one edge are antialigned to the spin moments on the opposite edge. Figure 7(b) shows the *ferromagnetic* (FM) configuration, where the spin moments on both edges point in the same direction.

Both the AF and FM configurations are found to have a total energy lower than the nonmagnetic state for all ribbon widths, indicating that spin polarization is a possible stabilization mechanism. The energy difference between the nonmagnetic and the antiferromagnetic states plotted in Fig. 8 is a measure of the strength of the magnetic instability. The
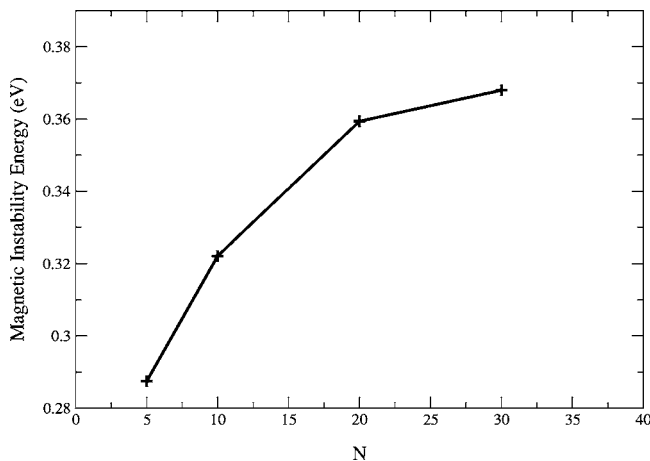

FIG. 8. The energy difference (per unit cell) between the nonmagnetic and antiferromagnetic case as a function of N.
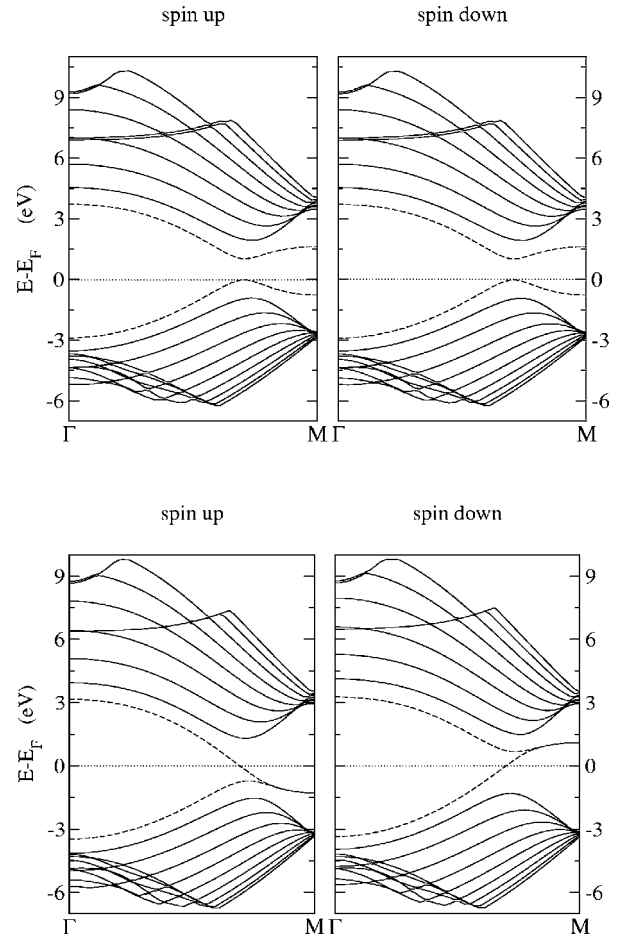

FIG. 9. Spin-polarized band structure of a $N=10$ ribbon. The antiferromagnetic case is shown in the upper panels and ferromagnetic case in the lower panels.

stabilization is larger for wider ribbons and converges to about 0.38 eV per unit cell at $N \sim 30$. Unlike the idealized system presented here, however, realistic systems are likely to present a mixture of zigzag and armchair edges. Since the armchair edges do not give rise to a high density of states at the Fermi level,[48] the magnetic instability computed here for the idealized system is likely to be overestimated with respect to the systems experimentally realized thus far.

The ground state of the system is found to be the AF case, as predicted by the spin alternation rule discussed elsewhere[39] and formally expressed in Lieb's theorem[49] in the framework of a Hubbard model. It is noteworthy that the spin alternation rule is satisfied also at the DFT level, which goes beyond the strictly on-site treatment of the electron-electron interaction of the Hubbard model. These results therefore extend the validity of the spin alternation rule beyond the approximations of the Hubbard model.

The analysis of the electronic structure and energetics of these two stable magnetic states as a function of the ribbon's width documents the range of the magnetic interaction between the edges and the nature of the stabilization mechanism via spin polarization. In Fig. 9 the band structures of the AF (upper panel) and FM (lower panel) states are presented. The instability of the nonmagnetic case discussed in

Sec. III A is resolved into two completely different but well-known scenarios: the AF solution gives a Slater insulator, while the FM solution gives a Stoner metal.

In the AF configuration, opposite spin polarization on neighboring sites localizes the electrons in singlet pairing between the two sublattices and a band gap opens at $k = \frac{2}{3}\frac{\pi}{a}$, where the valence and conduction bands of graphene are degenerate (Fig. 3). The electronic ground state of a mono-hydrogenated ribbon of finite width is therefore insulating. As the width increases, the band gap tends to zero following an algebraic decay of the type $1/N$ (as for the bulk gap of Fig. 6). The band gap vanishes, within the room-temperature thermal energy, when $N \simeq 400$, i.e., for an 80-nm width. This length scale could be reached by the nanotechonolgy industry in the future with the synthesis of single, relatively thin sheets of nanographite.

Conversely, in the case of the metastable FM configuration the spin-up and spin-down bands cross in a nonbonding fashion at E_F at $k = \frac{2}{3}\frac{\pi}{a}$. The states near E_F are delocalized in the middle of the ribbon, where no spin density is present. In contrast, a small amount of spin polarization and electron localization is present in the same region in the case of the AF configuration, indicating that the spin polarized nature of its edge states penetrates deeper into the bulk. The range of edge states and of the magnetic interactions will be discussed further in Sec. IV B. Notably, no significant difference is detected in the bulk bands of the nonmagnetic, AF and FM cases, indicating that magnetic effects on these bands are negligible. As the ribbon's width increases, the bulk bands closest to E_F approach each other and eventually become degenerate at $k = \frac{2}{3}\frac{\pi}{a}$, thus recovering the graphene band structure. The results of these calculation imply that as N goes to infinity the edges remain spin-polarized but, as it will be shown in the next subsection, no interedge magnetic order exists. The degree of spin polarization decays into the bulk and this remains an edge effect, not detectable by bulk-sensitive techniques. In this limit, the system is a zero band-bap semiconductor but the computed band structure is not identical to that of an infinite sheet of graphene because the edge states are still present at E_F. These states, however, decay into the bulk and only an edge-sensitive electronic probe would detect them. From a nanotechnological point of view, the AF and FM band structures show some appealing features. In fact, the prediction that at the nanometer level an AF alignment of the edges' spins produces a strongly insulating state and that a FM alignment is conducting implies that one is able to control the conducting properties of a nanosample by applying appropriately modulated magnetic fields.

By adopting a mean-field version of the Hubbard model with nearest-neighbor hopping, it is possible to estimate the values of the hopping integral t and of the on-site Coulomb repulsion parameter, usually referred to as the Hubbard U. This is achieved by fitting the computed band structure due to the edge states at E_F with that produced by the Hubbard model. The resulting values are $t \simeq 3.2$ eV and $U \sim 2t$. Note that this Hubbard U parameter, defined as the direct Coulomb integral between the nonbonding localized orbitals (of atomic nature, as for the d orbitals in transition-metal com-
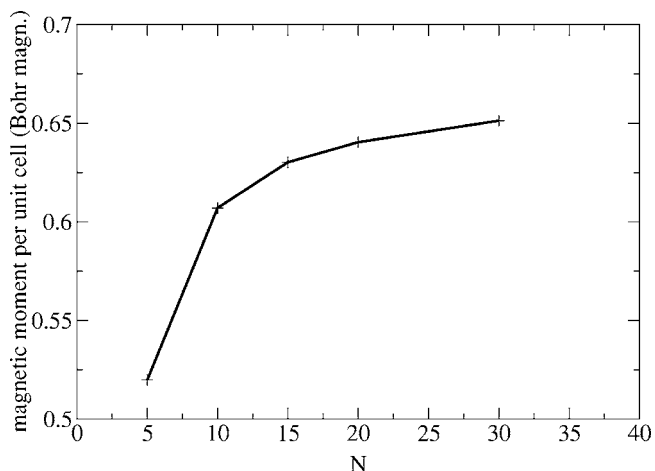

FIG. 10. The magnetic moment per unit cell as a function of the ribbon width in the ferromagnetic state.

pounds) that exist at the edges of graphene ribbons is not to be compared with the U parameter of an infinite graphene sheet where the π orbitals are always delocalized.

It is noteworthy that the values obtained for t and U depend on the choice of the exchange-correlation functional used within the DFT calculations. Within the gradient-corrected functional PBE,[25] one obtains $t \simeq 2.5$ eV and $U \sim 1.3t$, while the local-density approximation (LSDA) (Ref. 24) gives $t = 2.5$ eV and $U = 0.9t$.

These trends can be understood in terms of the approximation to the electronic exchange in the various functionals. The LSDA has a tendency to delocalize states and suffers from electron self-interaction which, in this context, results in a lower value for the Hubbard U parameter. The LSDA might therefore be expected to yield an overestimation of the hopping parameter t and an underestimation of U. The gradient-corrected PBE functional contains a somewhat better description of the semilocal exchange, which increases U but does not significantly affect t. The B3LYP functional contains an element of Fock exchange that explicity compensates for electronic self-interaction and therefore provides a significantly higher U, and tends to localize the electronic states much more than LSDA or PBE. As will be discussed in the next section, a higher degree of localization increases the strength of the magnetic interaction but decreases its range. As discussed above, B3LYP is likely to provide a more reliable description of this delicate balance but further studies of s-p bonded systems are required to establish this.

Figure 10 shows the magnetic moment per unit cell for the FM case which, as expected, approaches the saturation value of $2/3\mu_B$. As the ribbon widens, the covalent interaction between the tails of the edges' wave functions diminishes in favor of a purely ionic arrangement of the charge, which consists in $1/3e^-$ (for each edge atom) not participating in any bonding.

B. Range of magnetic interaction

As the AF and FM states differ by flipping the spin moments of one edge, the range of the magnetic interaction in
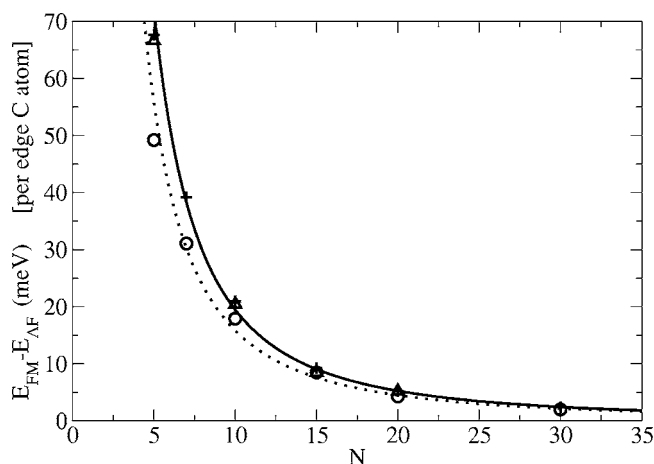
FIG. 11. The magnetic interaction strength as a function of ribbon's width. Empty circles refer to the monohydrogenated ribbon and are fitted using a power-law decay (dotted line) of $1/N^{1.82}$. The plus and triangle symbols refer to the methylene-group terminated and nonterminated ribbons whose decay laws are $1/N^{1.89}$ and $1/N^{1.86}$, respectively.
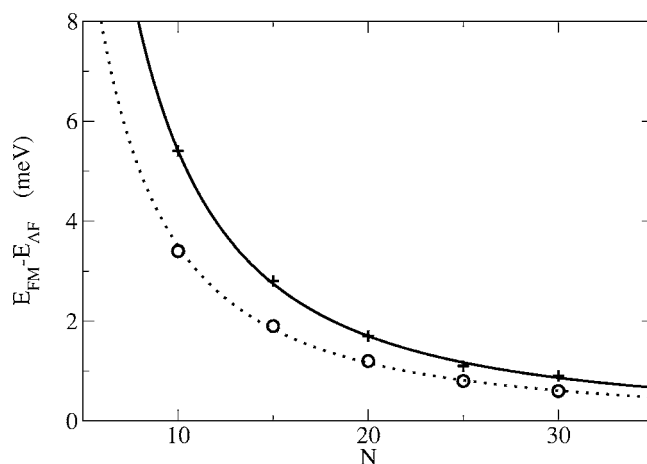

FIG. 12. Magnetic interaction strength as a function of ribbon's width within PBE (plus) and LSDA (circle). The decay power laws are, respectively, $1/N^{1.44}$ and $1/N^{1.39}$.

the ribbons can be measured by computing how the energy difference ΔE, between these two states varies as a function of the ribbon's width. The behavior of the B3LYP-computed ΔE as a function of the ribbon's width is plotted in Fig. 11 for the different types of termination described in Sec. II. The plot refers to unrelaxed ribbons (geometric relaxation has been found to affect ΔE only negligibly).

By fitting the energy variation with N, one obtains a decay law close to $1/N^2$ for each of the three different terminations considered here: the monohydrogenated, the methylene-group terminated, and the nonterminated ribbons. This establishes that the essential behavior in these systems is independent of the particular mechanism used to terminate the zigzag ribbon edge.

Irrespective of the termination type, a width of $N \sim 8$, corresponding to approximately $14–16$ Å, gives $\Delta E \simeq 25$ meV and thus room-temperature magnetic ordering. This value is significantly higher compared to previous studies based on standard DFT. In a recent LSDA study by Lee *et al.*,[50] the exchange interaction is reported to be less than 5 meV at $N = 8$. Moreover, Wakabayashi *et al.*[51] found a value smaller than 5 meV for $N = 3$ in their investigation of the spin-wave spectrum within the random-phase approximation of the Hubbard model. At $T = 0$ the energy difference between the AF and FM states remains non-negligible, within the accuracy of the present calculations, up to $N \sim 30$.

Figure 12 displays the same property computed for the monohydrogenated ribbons within the functionals PBE and LSDA. As noted in Sec. IV A, when calculating the Hubbard U the degree of charge localization is smaller in PBE and LSDA than in B3LYP; the magnetic tails of the edge states in PBE and LSDA are more delocalized and therefore more long-ranged. The delocalization of the state means that the strength of the interaction is lower than with B3LYP but its range is increased. The decay power law is $1/N^{1.44}$ within PBE and $1/N^{1.39}$ within LSDA. It is interesting to note that only very narrow ribbons could display room-temperature

magnetic order according to LSDA and PBE, while within B3LYP their width is predicted to extend to $1–2$ nm.

V. ELECTRONIC CHARGE POLARIZATION

The instability brought about by the high density of states at the Fermi level in the nonmagnetic ribbons could, in principle, also be resolved by a charge polarization mechanism. When the Hubbard model is extended to include off-site Coulomb interactions, for instance, the possibility of charge order appears. Recently, Yamashiro *et al.*[20] investigated the effect of nearest-neighbor interactions for a graphitic ribbon adopting an extended Hubbard model within the unrestricted Hartree-Fock (UHF) approximation. In their study it was found that for some values of the off-site parameter, the charge-polarized (CP) and spin-polarized states compete.

The possibility of a CP state is explored here for an $N = 10$ ribbon and within two levels of theory: UHF and B3LYP. In the case of UHF, a metastable CP state can be computed in which a charge transfer of about $0.05e^-$ occurs from the C atoms of one edge to those of the other. The spin-polarized state, however, is much more stable (by 1 eV per cell) than the CP state. In the case of B3LYP, different initial charge densities were tried, corresponding to charge transfers of 0.05 (as in the stable UHF solution) and $0.04e^-$. All such states, however, converge to the spin-polarized solution. If the proportion of Fock exchange included in the hybrid functional is increased from 20% (i.e., the percentage of Fock exchange present in B3LYP), a metastable CP state is only achieved at the extreme limit of 100%, which corresponds to UHF with a LYP treatment of correlation. It seems that this extreme limit produces an unphysical instabilty and indeed it is found that both the 100% Fock exchange functional and UHF theory predict the FM state to be the ground state for larger ribbon widths, which is inconsistent with all other results and clashes with Lieb's theorem and the spin alternation rule.

VI. DISCUSSION AND CONCLUSION

In this work, the possible stabilization mechanisms for a zigzag ribbon via geometric distortion, spin polarization, and

charge polarization have been investigated. The influence of the ribbon's width on the electronic structure and relative stability of the different solutions were also analyzed.

The topology of the nonbonding crystalline orbitals at the edges does not allow for a significant Peierls distortion for ribbons with N greater than 3 but rather an edge relaxation which preserves a strong tendency of the system to stabilize through a magnetic polarization, where magnetic moments are localized at the edges. Two magnetic states were investigated: (i) an antiferromagnetic configuration where the spin moments on the C atoms at one edge are antialigned to those on the other edge; (ii) a ferromagnetic configuration where all spin moments on the C atoms at the edges point in the same direction. Both states were found to be lower in energy than the nonmagnetic state for any width of the ribbons. The antiferromagnetic state was found to be the ground state in agreement with the spin alternation rule and extending Lieb's theorem beyond the nearest-neighbor approximation. This conclusion is expected to be robust with respect to structural defects that partially break the symmetry of the bipartite lattice since the spin alternation rule was found to hold for curved and defective (but still mainly $sp2$-bonded) systems such as fullerene solids with covalent intercage bonds, carbon vacancies, and chemisorbed hydrogen.[38–40] The range of the magnetic interaction, however, may be affected in a strongly defective system.

The magnetic state was found to be about 0.38 eV per unit cell more stable than the diamagnetic one for wide ribbons. In ribbons that have been realized thus far there is a mixture of zigzag and magnetically inactive edges which weaken the tendency towards a magnetic state. This is a possible explanation of the recent scanning tunneling spectroscopy experiment in which Niimi *et al.*[52] measured a peak in the local density of states (LDOS) of edge atoms signalling the existence of a nonmagnetic metallic state (Fig. 3). In fact, if the system were magnetic, the LDOS at the edge would have shown two symmetric peaks around the Fermi level representing the opening of a Hubbard gap due to the magnetic polarization of the π system, as discussed in Sec. IV.

By fitting the antiferromagnetic band structure to a nearest-neighbor Hubbard model the value of the U parameter associated with the localized states at the edges was found to be dependent on the exchange-correlation functional used. Going from PBE and LSDA to B3LYP the U value increases due to the explicit inclusion of a self-interaction correcting term in the DFT Hamiltonian. The self-interaction error is known to be the main cause of the failure of the LSDA and PBE in the treatment of systems containing localized d orbitals. However, it is not clear at present which treatment of exchange and correlation provides the most reliable approach for a system containing localized or atomic-like s-p orbitals.

The magnetic interaction strength was computed as a function of the ribbon width and, within the B3LYP functional, it was found that ribbons less than 1.5–2 nm across retain magnetic order above room temperature. Within LSDA and PBE the magnetic interaction strength is weaker but longer ranged. These three functionals provide differing descriptions of the interplay between localization and delocalization and its effect on the strength and range of the magnetic interaction. This is evident in the predicted critical ribbon width at which the magnetic state becomes thermally unstable at room temperature; B3LYP predicts a critical width of 1–2 nm while LSDA and PBE predict a width an order of magnitude smaller.

In conclusion, first-principles calculations have been used to establish that the electronic structure of graphene ribbons with zigzag edges is unstable with respect to a magnetic polarization of the edge states. This mechanism is stable with respect to alternative stablization routes involving charge polarization or structural distortions. The magnetic interaction of the edge states is remarkably long ranged. A band gap in the bulk of the ribbon exists in the antiferromagnetically aligned ground state with the size of the gap also displaying a very long-ranged dependence on the ribbon width closing, at room temperature for ribbon widths exceeding 80 nm. The qualitative features of these results are robust with respect to differing treatments of electronic exchange and correlation. This explicit demonstration of the long-ranged nature of the magnetic interaction mediated by the delocalized π orbitals in graphitic systems is consistent with recent observations of magnetism induced by low defect concentrations in a number of materials.[53] These results have direct implications for the control of the spin-dependent conductance in graphitic nanoribbons using suitably modulated magnetic fields. The practical feasibility of nanoribbon-based devices operating based on the properties addressed here is an important consideration. The practical realization of a nanoribbon with magnetic ordering requires a critical width of 10–20 Å which is challenging for the present nanotechnology industry. On the other hand, because the band gap of the AF state closes only at ∼800 Å, while the FM state remains always metallic, the realization of a nanoribbon device in which a metal-insulator transition can be induced by applying a suitably modulated magnetic field may be feasible at present.

[1] P. Esquinazi, D. Spemann, R. Höhne, A. Setzer, K.-H. Han, and T. Butz, Phys. Rev. Lett. **91**, 227201 (2003).

[2] J. Barzola-Quiquia, S. Petriconi, P. Esquinazi, M. Rothermel, D. Spemann, A. Setzer, and T. Butz, cond-mat/0610293 (unpublished).

[3] H. Ohldag, T. Tyliszczak, R. Hoehne, D. Spemann, P. Esquinazi, M. Ungureanu, and T. Butz, cond-mat/0609478 (unpublished).

[4] T. Butz, D. Spemann, K. H. Han, R. Hohne, A. Setzer, and P. Esquinazi, Hyperfine Interact. **160**, 27 (2005).

[5] A. V. Rode, E. G. Gamaly, A. G. Christy, J. G. Fitz Gerald, S. T. Hyde, R. G. Elliman, B. Luther-Davies, A. I. Veinger, J. Androulakis, and J. Giapintzakis, Phys. Rev. B **70**, 054407 (1999).

[6] P. Turek, K. Nozawa, D. Shiomi, K. Awaga, T. Inabe, Y. Maruyama, and M. Kinoshita, Chem. Phys. Lett. **180**, 327 (1991).

[7] V. I. Srdanov, G. D. Stucky, E. Lippmaa, and G. Engelhardt, Phys. Rev. Lett. **80**, 2449 (1998).

[8] T. Enoki and Y. Kobayashi, J. Mater. Chem. **15**, 3999 (2005).

[9] Y.-W. Son, M. Cohen, and S. G. Louie, Nature (London) **444**, 347 (2006).

[10] Y.-W. Son, M. L. Cohen, and S. G. Louie, Phys. Rev. Lett. **97**, 216803 (2006).

[11] M. Fujita, K. Wakabayashi, K. Nakada, and K. Kusakabe, J. Phys. Soc. Jpn. **65**, 1920 (1996).

[12] N. M. R. Peres, A. H. Castro Neto, and F. Guinea, Phys. Rev. B **73**, 195411 (2006).

[13] N. M. R. Peres, F. Guinea, and A. H. Castro Neto, Phys. Rev. B **73**, 125411 (2006).

[14] M. A. H. Vozmediano, M. P. Lopez-Sancho, T. Stauber, and F. Guinea, Phys. Rev. B **72**, 155121 (2005).

[15] T. Hikihara, X. Hu, H.-H. Lin, and C. Y. Mou, Phys. Rev. B **68**, 035432 (2003).

[16] K. Kusakabe and M. Maruyama, Phys. Rev. B **67**, 092406 (2003).

[17] K. Wakabayashi, M. Fujita, H. Ajiki, and M. Sigrist, Phys. Rev. B **59**, 8271 (1999).

[18] Y. Shibayama, H. Sato, T. Enoki, and M. Endo, Phys. Rev. Lett. **84**, 1744 (2000).

[19] D. Arcon, Z. Jaglicic, A. Zorko, A. V. Rode, A. G. Christy, N. R. Madsen, E. G. Gamaly, and B. Luther-Davies, Phys. Rev. B **74**, 014438 (2006).

[20] A. Yamashiro, Y. Shimoi, K. Harigaya, and K. Wakabayashi, Phys. Rev. B **68**, 193410 (1999).

[21] A. D. Becke, Phys. Rev. A **38**, 3098 (1988).

[22] A. D. Becke, J. Chem. Phys. **98**, 5648 (1993).

[23] C. Lee, W. Yang, and R. G. Parr, Phys. Rev. B **37**, 785 (1988).

[24] U. von Barth and L. Hedin, J. Phys. C **5**, 1629 (1972).

[25] J. P. Perdew, K. Burke, and M. Ernzerhof, Phys. Rev. Lett. **77**, 3865 (1996).

[26] W. E. Pickett, Rev. Mod. Phys. **61**, 433 (1989).

[27] W. C. Mackrodt, N. M. Harrison, V. R. Saunders, N. L. Allan, M. D. Towler, E. Apra, and R. Dovesi, Philos. Mag. A **68**, 653 (1993).

[28] M. Ernzerhof and G. E. Scuseria, J. Chem. Phys. **110**, 5029 (1999).

[29] J. Muscat, A. Wander, and N. M. Harrison, Chem. Phys. Lett. **342**, 397 (2001).

[30] R. L. Martin and F. Illas, Phys. Rev. Lett. **79**, 1539 (1997).

[31] T. Bredow and A. R. Gerson, Phys. Rev. B **61**, 5194 (2000).

[32] I. P. R. Moreira, F. Illas, and R. L. Martin, Phys. Rev. B **65**, 155102 (2002).

[33] J. K. Perry, J. Tahir-Kheli, and William A. Goddard III, Phys. Rev. B **63**, 144510 (2001).

[34] X. Feng and N. M. Harrison, Phys. Rev. B **70**, 092402 (2004).

[35] X.-B. Feng and N. M. Harrison, Phys. Rev. B **69**, 132502 (2004).

[36] X.-B. Feng and N. M. Harrison, Phys. Rev. B **69**, 035114 (2004).

[37] M. Schmidt, W. Ratcliff II, P. G. Radaelli, K. Refson, N. M. Harrison, and S. W. Cheong, Phys. Rev. Lett. **92**, 056402 (2004).

[38] J. A. Chan, B. Montanari, W. L. Chan, and N. M. Harrison, Mol. Phys. **103**, 2573 (2005).

[39] J. A. Chan, B. Montanari, J. D. Gale, S. M. Bennington, J. W. Taylor, and N. M. Harrison, Phys. Rev. B **70**, 041403(R) (2004).

[40] J. A. Chan, B. Montanari, and N. M. Harrison, in *Carbon-based Magnetism: An Overview of the Magnetism of Metal-free Carbon-based Compounds and Materials*, edited by T. Makarova and F. Palacio (Elsevier, Amsterdam, 2006), pp. 523–540.

[41] V. R. Saunders, R. Dovesi, C. Roetti, R. Orlando, C. M. Zicovich-Wilson, N. M. Harrison, K. Doll, B. Civalleri, I. J. Bush, Ph. D'Arco, and M. Llunell, *CRYSTAL2003 User's Manual* (University of Torino, Torino, 2003).

[42] H. B. Schelegel, J. Comput. Chem. **3**, 214 (1982).

[43] J. Demaison and G. Wlodarczak, Struct. Chem. **5**, 57 (1994).

[44] P. R. Wallace, Phys. Rev. **71**, 622 (1947).

[45] R. E. Peierls, *Quantum Theory of Solids* (Clarendon, Oxford, 1955).

[46] M. Kertesz and R. Hoffmann, Solid State Commun. **47**, 97 (1983).

[47] P. Ruffieux, O. Groning, P. Schwaller, L. Schlapbach, and P. Groning, Phys. Rev. Lett. **84**, 4910 (2000).

[48] K. Nakada, M. Fujita, G. Dresselhaus, and M. S. Dresselhaus, Phys. Rev. B **54**, 17954 (1996).

[49] E. H. Lieb, Phys. Rev. Lett. **62**, 1201 (1989).

[50] H. Lee, Y. Son, N. Park, S. Han, and J. Yu, Phys. Rev. B **72**, 174431 (2005).

[51] K. Wakabayashi, M. Sigrist, and M. Fujita, J. Phys. Soc. Jpn. **67**, 2089 (1997).

[52] Y. Niimi, T. Matsui, H. Kambara, K. Tagami, M. Tsukada, and H. Fukuyama, Phys. Rev. B **73**, 085421 (2006).

[53] J. M. D. Coey, SIAM (Soc. Ind. Appl. Math.) J. Sci. Stat. Comput. **7**, 660 (2005).